MATHEMATICAL MODELING AND COMPUTING, Vol. 12, No. 3, pp. 957–971 (2025)

Boundary layer flow and heat transfer towards a stretching or shrinking cylinder within carbon nanotubes with hydromagnetic effects

Sidin A. A. A.[1], Bachok N.[2], Wahid N. S.[2], Mustafa M. S.[2]

[1]*Institute for Mathematical Research, Universiti Putra Malaysia, 43400 UPM Serdang, Selangor, Malaysia*
[2]*Department of Mathematics and Statistics, Faculty of Science, Universiti Putra Malaysia, 43400 UPM Serdang, Selangor, Malaysia*

(Received 3 March 2025; Revised 28 September 2025; Accepted 29 September 2025)

The numerical investigation of stagnation point flow past a stretching or shrinking cylinder in carbon nanotubes with the presence of hydromagnetic effects is examined. This study has been solved by ordinary differential equations obtained using the similarity transformation that transformed from the governing equations along with the boundary conditions, then implemented the bvp4c solver in MATLAB software platform, ensuring accurate results. Considering two types of base fluids, namely water and kerosene. Also, single-wall and multi-wall types of carbon nanotubes are used in this study, with single-wall and multi-walled consisting of different values of density. The study is investigated by generating the graphical result of the velocity, temperature, skin friction coefficient and heat transfer rate. Several parameters are considered, such as magnetic field M, curvature parameter γ, stretching or shrinking parameter ε and nanoparticle volume fraction φ. From the numerical results, it is demonstrated that a non-unique solution exists for the shrinking parameter, while a unique solution is obtained for stretching parameter. Furthermore, single-walled carbon nanotubes and kerosene-based nanofluid are found to be more effective for heat transfer than multi-walled carbon nanotubes and water-based nanofluid. Response surface methodology (RSM) is utilized to optimize the heat transfer, with the heat transfer maximized for water-SWCNT estimated at 0.880135 and a desirability of 99.98% which is higher than water-MWCNT, indicating water-SWCNT is more effective.

Keywords: *heat transfer; stretching or shrinking cylinder; carbon nanotubes; optimization; dual solutions.*

2010 MSC: 35Q35, 35Q79, 62K20, 76D10, 76W05 **DOI:** 10.23939/mmc2025.03.957

1. Introduction

In recent years, there has been limited research focused on stretching or shrinking cylinders. However, these cylinders are utilized in various engineering fields such as biomedical engineering and chemical processing. They are utilized in biomechanics and tissue engineering studies, including research on blood vessels and muscles. Additionally, stretching or shrinking cylinder are employed in chemical reactors for vessel deformation and flow channel analysis. The study of stretching or shrinking cylinder can be founded by few authors, such as Wang [1] studied the fluid flow outside of a stretching cylinder. Mukhopadhyay [2] analyzed the flow and thermal characteristics of boundary layer axisymmetric flow along a stretching cylinder under the combined influence of slip and a uniform magnetic field. The findings of the study, it is found that the velocity decreases with increasing velocity slip parameter and magnetic parameter. The skin friction coefficient as well as the heat transfer rate at the surface is larger for a cylinder compared to a flat plate. Then, Najib et al. [3] investigated the stagnation point flow and mass transfer with chemical reaction past a stretching/shrinking cylinder. Next, axisymmetric flow of a viscous incompressible fluid over a shrinking vertical cylinder with heat transfer is investigated by Mishra and Singh [4]. Mat et al. [5] examined the boundary layer stagnation-point slip flow and heat

transfer along a shrinking/stretching cylinder over a permeable surface found that velocity and temperature profiles increase as the curvature parameter increases. Khashi'ie et al. [6] investigated hybrid nanofluid flow past a shrinking cylinder with prescribed surface heat flux and stated that flat plate surface abates the separation of boundary layer while it enhances the heat transfer process. Awaludin et al. [7] also shows an interest in study the steady stagnation point flow and heat transfer passes a horizontal shrinking permeable cylinder. It stated that given the existence of dual solutions in the present study for a certain range of the curvature parameter. Further studies on stretching/shrinking cylinders in nanofluids, such as Kardri et al. [8], examine MHD stagnation point flow and heat transfer over a nonlinear stretching/shrinking cylinder in nanofluids, accounting for viscous dissipation and heat generation using the Tiwari–Das model.

The term "nanofluid", which refers to a fluid containing nanoscale particles with a dimension of less than 100 nm, was originally used by Choi and Eastman [9]. Nanofluids have a significant impact on research applications owing to their enhanced thermal conductivity, which improves heat transfer rates and efficiency in heat exchange systems. Consequently, this capability can lead to the development of more compact and efficient heat exchangers, reduced energy consumption and enhanced overall system performance. Arifin et al. [10] expressed interest in investigating viscous flow induced by a permeable stretching/shrinking sheet in a nanofluid, an extension initially proposed by Wang [11] from the original work of Tiwari and Das [12]. Copper and silver are examined as nanoparticles to explore the impact of nanoparticle volume fraction on the flow and the characteristics of heat transfer. The explore of research in using nanofluid can be seen in the papers [13–16]. Carbon nanotubes (CNTs) have exceptionally high thermal conductivity as stated by Iijima [17], several times greater than copper or silver nanoparticles. This property makes them highly effective in enhancing heat transfer rates in nanofluids, leading to improved thermal management in various systems. It was stated by Halelfadl et al. [18] that nanofluids could offer advantages in energy systems and heat exchangers where fluid flow aligns with the setup's temperature, the volume fraction of nanoparticles and flow regimes. Few studies have explored the use of carbon nanotubes, for example, Anuar et al. [19] studied nonlinear stretching/shrinking by implementing the influence of hydromagnetics.

Few studies have considered the effects of magnetohydrodynamics. Mahapatra et al. [20] explored the steady two-dimensional stagnation-point flow of an incompressible viscous electrically conducting fluid toward a stretching surface, with the flow permeated by a uniform transverse magnetic field. Subsequently, Aman et al. [21] examined stagnation point flow past a stretching/shrinking sheet with the availability of magnetohydrodynamic effect and slip effect. They obtained results indicating that the presence of slip effects causes the skin friction coefficient to decrease and the heat transfer rate to increase. The main objective was to observe the non-unique solution, which was found to exist for a shrinking sheet, while a unique solution was observed for a stretching sheet. Other researchers have shown interest in considering magnetic field effects on stagnation point flow in their research, as evidenced [22–25]. Moreover, some studies consider MHD in the flow of stretching/shrinking sheets; for instance, Sama et al. [26] conducted research indicating that SWCNTs are more efficient than MWCNTs in heat transfer. Other studies considering CNTs on various surfaces of stretching/shrinking can be referenced from Anuar et al. [27] and Norzawary et al. [28].

This study employs Response Surface Methodology (RSM) to optimize the heat transfer rate. The use of RSM has been observed in a several studies addressing various problems. For instance, Shirvan et al. [29] conducted a study on the effects of independent parameters on the combined natural convection and surface radiation heat transfer in a cavity. Nevertheless, Mahanthesh et al. [30] designed a numerical experiment using a face-centered composite design (CCD) to explore the RSM technique for optimizing the heat transfer of hybrid nanomaterials. Subsequently, Mahanthesh et al. [31] also utilized RSM to optimize mass transfer by analyzing the Sherwood number. Yahaya et al. [32] used RSM to optimize heat transfer and investigate parameters that positively impact the response. The results obtained show a desirability of 99.99%, indicating that the optimized conditions in the study are almost perfect according to the ideal target and are highly satisfactory.

The objective of this study is to investigate the stagnation point flow past a linear stretching/shrinking cylinder in carbon nanotubes with magnetohydrodynamics effects. This research combines ideas from Anuar et al. [19], Kardri et al. [8] and Sama et al. [26] and represents a novel investigation with no prior studies on this specific topic. The governing equations are transformed into ordinary differential equations using the similarity variable to numerically solve. Several influential parameters are considered to investigate the effects on heat transfer rate, which are presented in graphical results. Response Surface Methodology (RSM) will also be performed to demonstrate the accuracy of the results and their impact on heat transfer.

2. Problem formulation

A steady carbon nanotube's flow in a linearly stretching/shrinking cylinder in the stagnation point region with the presence of magnetohydrodynamics (MHD) are examine in this study. Both single-walled and multi-walled carbon nanotubes serve as nanoparticles dispersed within two base fluids, water and kerosene. It is assumed that the free stream velocity is $U_\infty = bx$, with radius R placed in the incompressible nanofluid of constant temperature T_w and b is a constant. The stretching/shrinking velocity is written as $U_w = ax$, where a is a constant. Meanwhile, an external magnetic field is included in this problem with $M = \sigma B_o^2/\rho_{nf} b$, where B_o is a constant from Othman et al. [33]. The governing equations of continuity, momentum and energy can be written as follows:

$$\frac{\partial(ru)}{\partial x} + \frac{\partial(rv)}{\partial r} = 0, \tag{1}$$

$$u\frac{\partial u}{\partial x} + v\frac{\partial u}{\partial r} = U_\infty \frac{dU_\infty}{dx} + \left(\frac{\mu_{nf}}{\rho_{nf}}\right)\left(\frac{\partial^2 u}{\partial r^2} + \frac{1}{r}\frac{\partial u}{\partial r}\right) + \frac{\sigma B^2}{\rho_{nf}}(U_\infty - u), \tag{2}$$

$$u\frac{\partial T}{\partial x} + v\frac{\partial T}{\partial r} = \alpha_{nf}\left(\frac{\partial^2 T}{\partial r^2} + \frac{1}{r}\frac{\partial T}{\partial r}\right), \tag{3}$$

and the following boundary conditions are

$$\begin{aligned} u = U_w, \quad v = 0, \quad T = T_w \quad \text{at} \quad r = R, \\ u \to U_\infty, \quad T \to T_\infty \quad \text{as} \quad r \to \infty, \end{aligned} \tag{4}$$

given that the velocity components, u and v are in the x and r directions, respectively and T denoted for fluid temperature. In Equation (5), it is demonstrated that the subscripts nf, f and CNT denote nanofluids, fluids and carbon nanotubes, respectively. Additionally, α represents the thermal diffusivity, μ stands for dynamic viscosity, ρ for the density, C_p signifies specific heat at constant pressure, k denotes thermal conductivity and φ indicates nanoparticle volume fraction, as illustrated below:

$$\begin{aligned} \alpha_{nf} = \frac{k_{nf}}{(\rho C_\rho)_{nf}}, \quad \mu_{nf} = \frac{\mu_f}{(1-\varphi)^{2.5}}, \quad \rho_{nf} = (1-\varphi)\rho_f + \varphi\rho_{CNT}, \\ (\rho C_p)_{nf} = (1-\varphi)(\rho C_p)_f + \varphi(\rho C_p)_{CNT}, \\ \frac{k_nf}{k_f} = \frac{1 - \varphi + 2\varphi\frac{k_{CNT}}{k_{CNT}-k_f}\ln\frac{k_{CNT}+k_f}{2k_f}}{1 - \varphi + 2\varphi\frac{k_f}{k_{CNT}-k_f}\ln\frac{k_{CNT}+k_f}{2k_f}} \end{aligned} \tag{5}$$

Based on Table 1, the thermophysical properties of SWCNT and MWCNT are compared across different base fluids: water and kerosene. These fluids were selected for comparison with previous studies. Additionally, the following similarity transformations in Equation (6) are introduced to solve the governing equations and the boundary conditions, ensuring satisfaction of the continuity Equation (1),

$$\eta = \frac{r^2 - R^2}{2R}\left(\frac{b}{v_f}\right)^{\frac{1}{2}}, \quad \psi = (bv_f)^{\frac{1}{2}} xRf(\eta), \quad \theta(\eta) = \frac{T - T_\infty}{T_w - T_\infty}, \quad v_f = \frac{\mu_f}{\rho_f}. \tag{6}$$

The governing equations of the momentum and energy equations from Equations (2) and (3) are simplified into ordinary differential equations (ODEs) through the utilization of Equation (5), employing the similarity transformations outlined in Equation (6), yielding the subsequent ODE and boundary

Table 1. Thermophysical properties of CNTs.

Physical properties	Based fluids		Nanoparticle	
	Water (Pr = 6.2)	Kerosene (Pr = 21)	SWCNT	MWCNT
ρ (kg/m^3)	997	783	2600	1600
c_p (J/(kg K))	4179	2090	425	796
k (W/(m K))	0.613	0.145	6600	3000

conditions form:

$$\frac{1}{(1-\varphi)^{2.5}[(1-\varphi)+\varphi\rho_{CNT}/\rho_f]}\left[(1+2\gamma\eta)f'''+2\gamma f''\right]+ff''-f'^2+M(1-f')+1=0, \tag{7}$$

$$\frac{1}{\Pr}\frac{k_{nf}/k_f}{[(1-\varphi)+\varphi(\rho\,C_\rho)_{CNT}/(\rho\,C_\rho)_f]}\left[(1+2\gamma\eta)\theta''+2\gamma\theta'\right]+f\,\theta'-f'\theta=0, \tag{8}$$

$$f(0)=0,\quad f'(0)=\varepsilon,\quad \theta(0)=1,\quad f'(\eta)\to 1,\quad \theta(\eta)\to 0,\quad \text{as}\quad \eta\to\infty, \tag{9}$$

where Pr represents the Prandtl number, M resembles magnetic field parameter and γ denotes the curvature parameter. The parameter for the shrinking/stretching surface is designated as ε, where $\varepsilon>0$ corresponds to the stretching case while $\varepsilon<0$ corresponds to the shrinking case,

$$\Pr=\frac{v_f}{\alpha_f},\quad M=\frac{\sigma B_o^2}{\rho_{nf}b},\quad \gamma=\left(\frac{v_f x^{(1-n)}}{bR^2}\right)^{\frac{1}{2}}. \tag{10}$$

The physical quantities of interest in this study are the skin friction coefficient, C_f and local Nusselt number, Nu_x, are given by:

$$C_f=\frac{\tau_w}{\rho_f {U_\infty}^2},\quad \mathrm{Nu}_x=\frac{xq_w}{k_f(T_w-T_\infty)}. \tag{11}$$

The shear stress of the surface T_w and heat flux q_w are notes as below:

$$\tau_w=\mu_{nf}\left(\frac{\partial u}{\partial r}\right)_{r=R},\quad q_w=-k_{nf}\left(\frac{\partial T}{\partial r}\right)_{r=R}. \tag{12}$$

By using Equation (10), the physical quantities in Equation (11) reduced to

$$\mathrm{Re}_x{}^{\frac{1}{2}}C_f=\frac{1}{(1-\varphi)^{2.5}}f''(0),\quad \mathrm{Re}_x{}^{-\frac{1}{2}}\mathrm{Nu}_x=-\frac{k_{nf}}{k_f}\theta'(0), \tag{13}$$

where $\mathrm{Re}_x=U_\infty x/v_f$ refers to the local Reynolds number.

3. Numerical analysis

Numerical solutions of the nonlinear ordinary differential equations (ODEs) Equations (7) and (8), along with boundary conditions Equation (9), were obtained using the boundary value problem solver (bvp4c) in MATLAB. Based on Table 2, the values of the $f''(0)$ can be compared between the study by Anuar et al. [19] and current study, considering $\gamma=\varphi=M=0$ for water-SWCNT. The consistent results obtained for $\gamma=0$ in both studies indicate validation, with both results being compatible. According to Anuar et al. [19], dual solutions can be found within the range of parameter influences such as $0.1\leqslant\varphi\leqslant 0.2$ and Kardri et al. [8] suggested that the value of γ is in range of $0\leqslant\gamma\leqslant 0.4$. However, after multiple attempts to generate the graphs within that range, it was observed that no solution exists for large values of γ. Hence, to obtain dual solution, the range of γ needs to be less than 0.1, specifically within $0\leqslant\gamma\leqslant 0.02$. This study also considers stretching or shrinking cases with the parameter ε. As can be seen in Table 1, it provides a comprehensive overview of the thermophysical characteristics of both types of carbon nanotube with two base fluids: water and kerosene. This includes their respective values for density, specific heat at constant temperature and thermal conductivity. In addition, this study contributes to the determination of the Prandtl number, which exhibits variability based on the chosen base fluids. Specifically, Pr is defined as Pr = 6.2 for water and Pr = 21 for kerosene.

Table 2. Values of $f''(0)$ for different ε and γ when $\varepsilon = M = 0$ for water-SWCNT.

ε	Anuar et al. [19]	Present results		
	$\gamma = 0$	$\gamma = 0$	$\gamma = 0.01$	$\gamma = 0.02$
2	−1.887307	−1.887307	−1.891910	−1.896505
1	0	0	0	0
0.5	0.713295	0.713295	0.715845	0.718387
0	1.232588	1.232588	1.238042	1.243475
−0.5	1.495670	1.495670	1.504878	1.514029
−1.0	1.328817	1.328817	1.345669	1.362272
−1.15	1.082231	1.082231	1.107213	1.131379
	[0.116702]	[0.116702]	[0.105222]	[0.094413]
−1.2	0.932473	0.932473	0.965974	0.997447
	[0.233650]	[0.233650]	[0.213369]	[0.195019]
−1.2465	0.584282	0.584281	0.721074	0.786771
	[0.554296]	[0.554296]	[0.430615]	[0.377963]

Figures 1 and 2 exhibit the variation of $f''(0)$ and $-\theta'(0)$, for different values of the curvature parameter γ along the stretching/shrinking parameter ε for water-MWCNT, for several values of γ when $M = 0.02$ and $\varphi = 0.1$. The reduced skin friction coefficient increases while the reduced heat transfer decreases as Oi increases in value. Additionally, the critical values ε_c also decrease. The dual solutions exist for $\varepsilon_c < \varepsilon \leqslant -1.0$ and unique solution only exist when $\varepsilon > -1.0$. Since, $\varepsilon > 0$ represents a stretching case, while $\varepsilon < 0$ represents a shrinking case, it can be concluded that dual solutions exist in the shrinking case, while uniqueness exists in the stretching case.

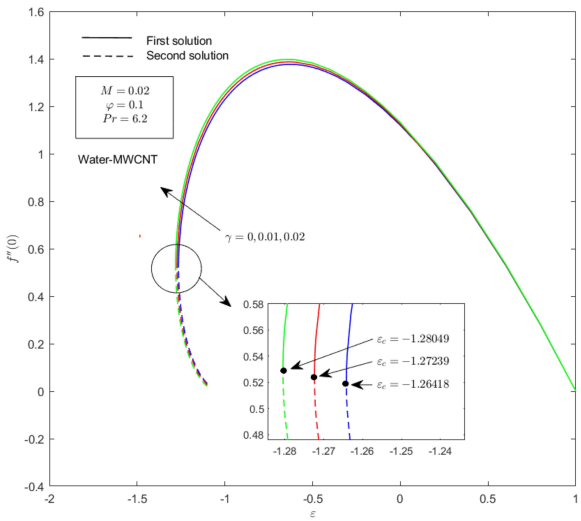

Fig. 1. Reduced skin friction coefficient $f''(0)$ for different γ.

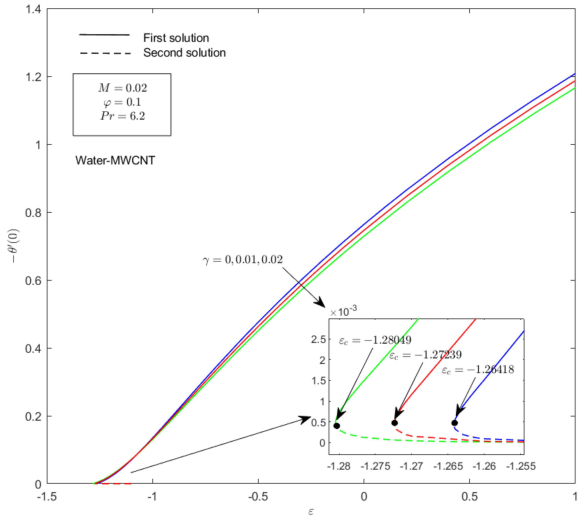

Fig. 2. Reduced heat transfer $-\theta'(0)$ for different γ.

The variations of skin friction coefficient $\mathrm{Re}_x{}^{\frac{1}{2}} C_f$ and local Nusselt number $\mathrm{Re}_x{}^{-\frac{1}{2}} \mathrm{Nu}_x$ with nanoparticle volume fraction are provided in Figures 3 and 4, with the different values of γ and different types of based fluid with single-walled carbon nanotube (SWCNT), specifically water-SWCNT and kerosene-SWCNT, within a shrinking case ($\varepsilon = -1.2$). The graphical results in Figures 3 and 4 illustrate the outcomes of the skin friction coefficient for different values of γ when $M = 0.02$. The value $\gamma = 0.01$ and 0.02 are taken to represent existence of the curvature parameter, while $\gamma = 0$ represents a flat surface. From Figure 3, it is shown that the kerosene-based fluid with single-wall CNTs causes the skin friction coefficient to increase. In Figure 4, it is revealed that the water-based fluid with single-wall CNTs contributes more significantly to heat transfer rate than the kerosene-based fluid with single-wall CNTs, primarily due to the influence of the curvature parameter.

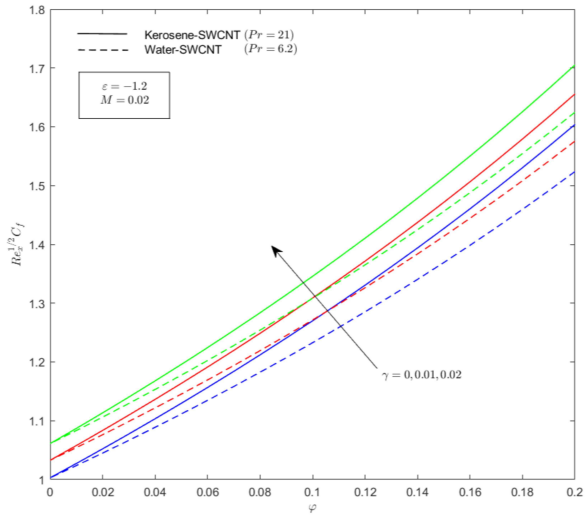

Fig. 3. Effect of γ on skin friction coefficient for single-walled CNTs.

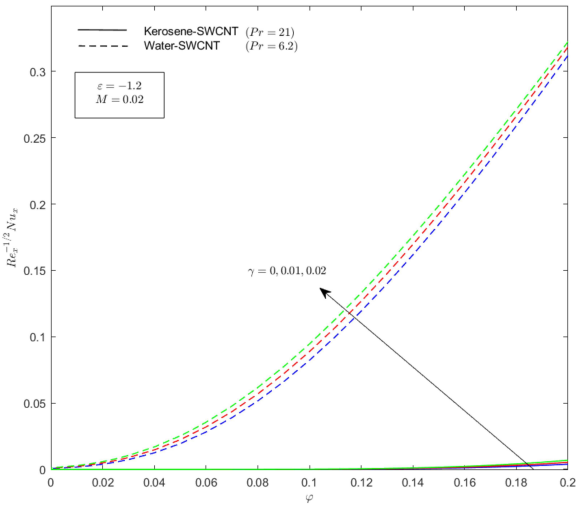

Fig. 4. Effect of γ on local Nusselt number for single-walled CNTs.

Furthermore, Figures 5 and 6 display the graphical results for the comparison of different based fluids with single-walled CNTs. Kerosene yields much higher skin friction coefficients than water, while the results for the local Nusselt number are opposite, with increasing values of M, water demonstrates significantly higher in local Nusselt number compared to kerosene.

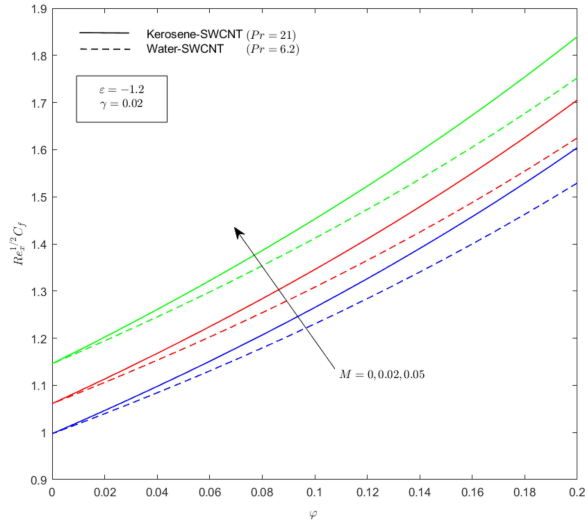

Fig. 5. Effect of M on skin friction coefficient for single-walled CNTs.

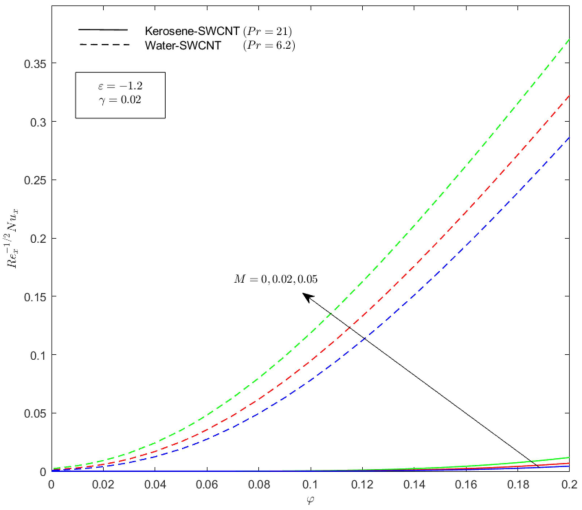

Fig. 6. Effect of M on local Nusselt number for single-walled CNTs.

Figures 7 and 8 display the impact of nanoparticle volume fraction φ and curvature parameter γ on velocity and temperature profiles. The curvature parameter is varied, with $\gamma = 0$ representing a flat surface and $\gamma = 0.01$ representing the presence of curvature. The influence of curvature parameter γ affects the velocity to be higher and the temperature profiles to be lower than those on the flat surface ($\gamma = 0$). It is observed from the figures that an increase in volume fraction of nanoparticles leads to a decrease in velocity profiles and an increase in the temperature profiles of the flow. This occurs because the increase in nanoparticle volume is associated with a decrease in the thickness of the velocity boundary layer adjacent to the walls, due to higher friction. Additionally, it enhances the thermal conductivity of the flow, resulting in an increase in temperatures.

In Figures 9 and 10 the figures demonstrate $f'(\eta)$ and $\theta(\eta)$ with the effects of different based fluids and type of carbon nanotubes (CNTs). The based fluids considered are water and kerosene, while

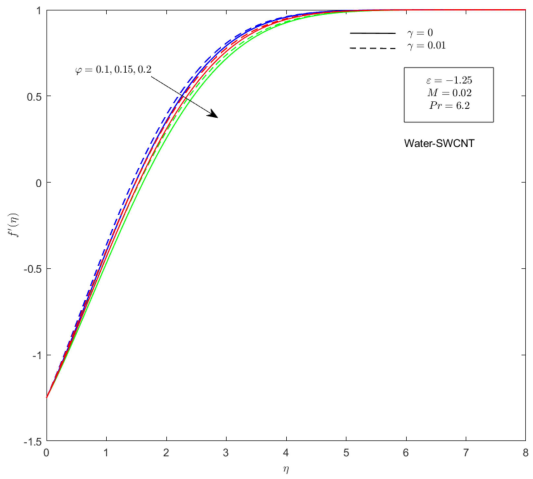

Fig. 7. Velocity profile for different value of φ and γ.

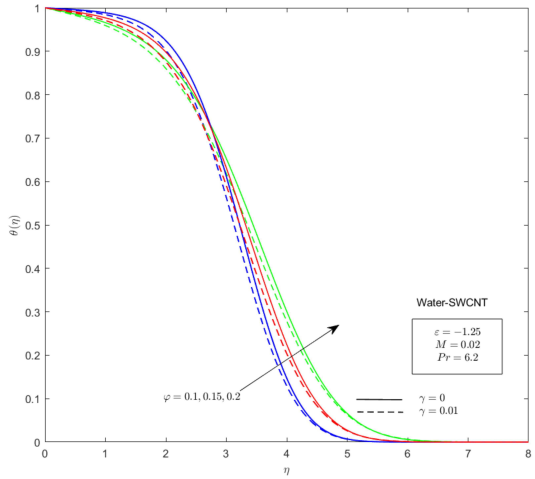

Fig. 8. Temperature profile for different value of φ and γ.

both single-wall (SWCNT) and multi-wall (MWCNT) CNTs are examined. It is evident that kerosene-SWCNT exhibits the highest velocity profiles, albeit slightly lower temperature profiles. Conversely, water-MWCNT shows the opposite trend compared to kerosene-SWCNT, with water-MWCNT displaying lower velocity profiles and higher temperature profiles. This proves that kerosene contributes to higher velocity profiles compared to water and single-wall CNTs produce higher velocity profiles than multi-wall CNTs. Additionally, since $\varepsilon < 0$ is considered, which corresponds to the shrinking case, dual solutions are present in both figures.

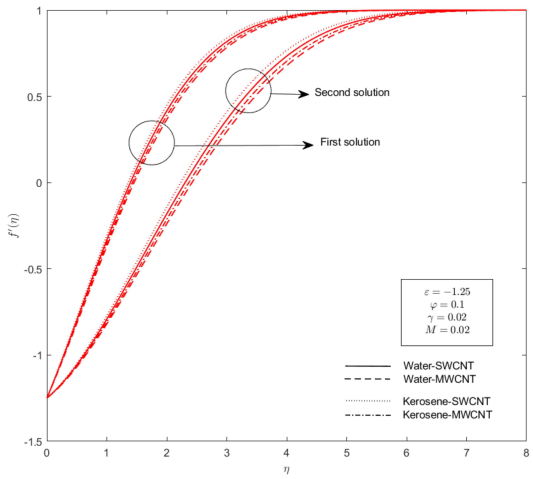

Fig. 9. Velocity profile for different nanoparticles.

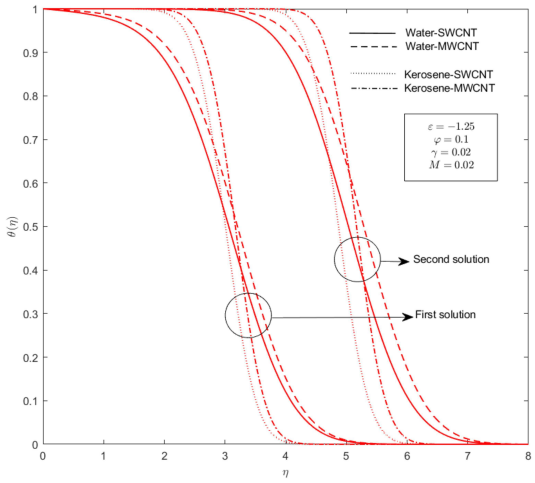

Fig. 10. Temperature profile for different nanoparticles.

4. Statistical analysis: Response surface methodology (RSM)

The technique of Response Surface Methodology (RSM) was founded in 1951 by George E. P. Box and K. B. Wilson. This technique is applied to explore the relationships among multiple explanatory variables and response variables. Moreover, the tools used in RSM are widely employed to obtain an optimal response, important properties and features such as orthogonality, rotatability and uniformity and are also utilized to maximize the result. Three parameters that are significantly connected to the heat transfer rate are evaluated. The relationship between the independent variables and the response is derived from Mahanthesh et al. [31]. The equation is expressed as follows:

$$Res = F(X_1, X_2, \ldots, X_t) \pm Er, \tag{14}$$

where Res and F respectively represent the response variable and unknown function of response. The variables $X_1, X_2, \ldots, X_t$ are the independent variables, while the statistical error is denoted by Er. Consequently, the quadratic model embedding is delineated as follows:

$$Res = a_0 + \sum_{i=1}^{t} a_i x_i + \sum_{i=1}^{t} a_{ii} x_i^2 + \sum_{i=1}^{t-1} \sum_{j=1}^{t} a_{ij} x_i x_j, \tag{15}$$

where intercept term (a_0), linear terms (a_i), bilinear two-factor terms (a_{ij}) and quadratic terms (a_{ii}).

Three factors were considered in this study for RSM to analyze the influence of parameters magnetic field M, nanoparticle volume fraction φ and curvature γ in optimizing the heat transfer rate which denoted as $\mathrm{Re}_x^{-\frac{1}{2}}\mathrm{Nu}_x$. The levels of each M, φ and γ along with their coded symbol x_1, x_2, x_3, respectively, are detailed in Table 3, representing low-level (-1), medium-level (0) and high-level (1). Utilizing the data from Table 4, numerical results are generated for the heat transfer coefficients of water-based fluids, considering both types of carbon nanotubes which is water-SWCNTs y_{SWCNT} and water-MWCNTs y_{MWCNT}. Thus, the quadratic model for the heat transfer of carbon nanotubes y_{CNT} constructed as below, employing the general quadratic model Equation (2):

$$y_{CNT} = a_0 + a_1 M + a_2 \varphi + a_3 \gamma + a_{11} M^2 + a_{22} \varphi^2 + a_{33} \gamma^2 + a_{12} M\varphi + a_{13} M\gamma + a_{23} \varphi\gamma. \tag{16}$$

Equation above with stated the intercept term (a_0), linear terms (a_i), bilinear two-factor terms (a_{ij}) and quadratic terms (a_{ii}), which get from Mahanthesh et al. [31]. The numerical experiment employs the face-centered CCD (central composite design), determined as $2^N + 2N + D$, where $D = 3$ denotes the number of factors and $N = 6$ represents the centre points. Thus, the design, consisting of three variables with three ranges involves 20 runs as can be seen in Table 4.

Table 3. Independent parameters and the range.

Parameters	Coded symbols	Levels		
		Low [-1]	Medium [0]	High [1]
M	x_1	0.01	0.03	0.05
φ	x_2	0.1	0.15	0.2
γ	x_3	0.01	0.015	0.02

Table 4. Experimental design.

Runs	Coded Symbols			Real Values			Responses	
	x_1	x_2	x_3	M	φ	γ	y_{SWCNT}	y_{MWCNT}
1	-1	-1	-1	0.01	0.1	0.01	0.410410849	0.326109371
2	1	-1	-1	0.05	0.1	0.01	0.439843033	0.352999785
3	-1	1	-1	0.01	0.2	0.01	0.839593417	0.645236869
4	1	1	-1	0.05	0.2	0.01	0.880231141	0.683151965
5	-1	-1	1	0.01	0.1	0.02	0.402840866	0.321528109
6	1	-1	1	0.05	0.1	0.02	0.430872486	0.347142881
7	-1	1	1	0.01	0.2	0.02	0.811547114	0.626400831
8	1	1	1	0.05	0.2	0.02	0.849920061	0.662111168
9	-1	0	0	0.01	0.15	0.015	0.616981715	0.481176429
10	1	0	0	0.05	0.15	0.015	0.651745672	0.513238718
11	0	-1	0	0.03	0.1	0.015	0.421215915	0.337142508
12	0	1	0	0.03	0.2	0.015	0.845564965	0.654481237
13	0	0	-1	0.03	0.15	0.01	0.643606740	0.503418220
14	0	0	1	0.03	0.15	0.02	0.625889021	0.491578475
15	0	0	0	0.03	0.15	0.015	0.634683989	0.497475140
16	0	0	0	0.03	0.15	0.015	0.634683989	0.497475140
17	0	0	0	0.03	0.15	0.015	0.634683989	0.497475140
18	0	0	0	0.03	0.15	0.015	0.634683989	0.497475140
19	0	0	0	0.03	0.15	0.015	0.634683989	0.497475140
20	0	0	0	0.03	0.15	0.015	0.634683989	0.497475140

The information in Table 4 was obtained using MATLAB software to obtain the responses of each parameter within a specific range. Subsequently, these data were utilized in Minitab Statistical Software to apply the RSM technique and generate the ANOVA tables as depicted in Tables 5 and 6 for the full model ANOVA of y_{SWCNT} and y_{MWCNT}. The presence of the symbol '$*$' indicates that the acquired data were too small for visualization. Alhadri et al. [34] emphasized that a parameter is considered statistically significant if its associated p-value is below 0.05, representing a significance level of 95%. The ANOVA analysis for both Table 7 and 8 revealed that the factors $x_1{*}x_1$ and $x_3{*}x_3$ were omitted from the full models of ANOVA for y_{SWCNT} and y_{MWCNT} due to their high p-value (> 0.05), suggesting insignificance in correlation with the response variable. All data underwent secondary validation via ANOVA until achieving a p-value less than 0.05.

Table 5. Analysis of variance (ANOVA) of y_{SWCNT}.

Source	DF	Adj SS	Adj MS	F-Value	P-Value
Model	9	0.454229	0.050470	758107.91	0.000
Linear	3	0.453940	0.151313	2272877.83	0.000
x_1	1	0.002932	0.002932	44045.49	0.000
x_2	1	0.450150	0.450150	6761703.49	0.000
x_3	1	0.000858	0.000858	12884.50	0.000
Square	3	0.000010	0.000003	52.47	0.000
$x_1{*}x_1$	1	0.000000	0.000000	4.02	0.073
$x_2{*}x_2$	1	0.000005	0.000005	68.22	0.000
$x_3{*}x_3$	1	0.000000	0.000000	0.22	0.652
2-Way interaction	3	0.000278	0.000093	1393.42	0.000
$x_1{*}x_2$	1	0.000058	0.000058	871.72	0.000
$x_1{*}x_3$	1	0.000002	0.000002	25.23	0.001
$x_2{*}x_3$	1	0.000219	0.000219	3283.31	0.000
Error	10	0.000001	0.000000		
Lack-of-Fit	5	0.000001	0.000000	*	*
Pure error	5	0.000000	0.000000		
Total	19	0.454229			

Table 6. Analysis of variance (ANOVA) of y_{MWCNT}.

Source	DF	Adj SS	Adj MS	F-Value	P-Value
Model	9	0.254756	0.028306	643220.18	0.000
Linear	3	0.254574	0.084858	1928282.50	0.000
x_1	1	0.002502	0.002502	56865.86	0.000
x_2	1	0.251685	0.251685	5719203.04	0.000
x_3	1	0.000386	0.000386	8778.62	0.000
Square	3	0.000016	0.000005	123.67	0.000
$x_1 * x_1$	1	0.000000	0.000000	4.26	0.066
$x_2 * x_2$	1	0.000008	0.000008	171.55	0.000
$x_3 * x_3$	1	0.000000	0.000000	0.05	0.820
2-Way interaction	3	0.000166	0.000055	1254.36	0.000
$x_1 * x_2$	1	0.000056	0.000056	1267.03	0.000
$x_1 * x_3$	1	0.000002	0.000002	34.41	0.000
$x_2 * x_3$	1	0.000108	0.000108	2461.64	0.000
Error	10	0.000000	0.000000		
Lack-of-Fit	5	0.000000	0.000000	*	*
Pure error	5	0.000000	0.000000		
Total	19	0.254757			

$$y_{SWCNT} = 0.634633 + 0.017124M + 0.212167\varphi - 0.009262\gamma - 0.001429\varphi * \varphi + 0.002693M * \varphi - 0.000458M * \gamma - 0.005227\varphi * \gamma, \quad (17)$$

$$y_{MWCNT} = 0.497426 + 0.015819M + 0.158646\varphi - 0.006215\gamma - 0.001796\varphi * \varphi + 0.002640M * \varphi - 0.000435M * \gamma - 0.003680\varphi * \gamma. \quad (18)$$

Table 7. Analysis of variance (ANOVA) for the reduced model of y_{SWCNT}.

Source	DF	Adj SS	Adj MS	F-Value	P-Value
Model	7	0.454228	0.064890	828859.55	0.000
Linear	3	0.453940	0.151313	1932777.24	0.000
x_1	1	0.002932	0.002932	37454.78	0.000
x_2	1	0.450150	0.450150	5749920.40	0.000
x_3	1	0.000858	0.000858	10956.54	0.000
Square	1	0.000010	0.000010	130.37	0.000
$x_2{}^*x_2$	1	0.000010	0.000010	130.37	0.000
2-Way interaction	3	0.000278	0.000093	1184.91	0.000
$x_1 * x_2$	1	0.000058	0.000058	741.28	0.000
$x_1 * x_3$	1	0.000002	0.000002	21.45	0.001
$x_2 * x_3$	1	0.000219	0.000219	2792.01	0.000
Error	12	0.000001	0.000000		
Lack-of-Fit	7	0.000001	0.000000	*	*
Pure error	5	0.000000	0.000000		
Total	19	0.454229			

Table 8. Analysis of variance (ANOVA) for the reduced model of y_{MWCNT}.

Source	DF	Adj SS	Adj MS	F-Value	P-Value
Model	7	0.254756	0.036394	679645.58	0.000
Linear	3	0.254574	0.084858	1584708.46	0.000
x_1	1	0.002502	0.002502	46733.72	0.000
x_2	1	0.251685	0.251685	4700177.20	0.000
x_3	1	0.000386	0.000386	7214.48	0.000
Square	1	0.000016	0.000016	301.12	0.000
$x_2 * x_2$	1	0.000016	0.000016	301.12	0.000
2-Way interaction	3	0.000166	0.000055	1030.86	0.000
$x_1 * x_2$	1	0.000056	0.000056	1041.27	0.000
$x_1 * x_3$	1	0.000002	0.000002	28.28	0.000
$x_2 * x_3$	1	0.000108	0.000108	2023.03	0.000
Error	12	0.000001	0.000000		
Lack-of-Fit	7	0.000001	0.000000	*	*
Pure error	5	0.000000	0.000000		
Total	19	0.254757			

As depicted in Figures 11 and 12, the contour and surface plots were generated for analysis. In relation to the linear terms discussed earlier, parameters M and γ have a negative impact on both y_{SWCNT} and y_{MWCNT}, while parameter φ has a positive effect on the response. These figures demonstrate that decreasing values of $x_1(M)$ and increasing values of $x_3(\gamma)$ lead to reduce in the response. Thus, with a high value of $x_1(M)$ and small value of $x_3(\gamma)$ results in a higher value of response. Hence, elevating the nanoparticle volume fraction parameter, φ, enhances the heat transfer rate.

It is possible to determine the optimum values of y_{SWCNT} and y_{MWCNT}. The examination of the influence of these parameters on optimizing the heat transfer rate is conducted through optimization using Response Optimizer with the goal of maximize and the results are presented in Tables 9 and 10. The optimization process aims to achieve the maximum value of $\mathrm{Re}_x^{-\frac{1}{2}}\mathrm{Nu}_x$, signifying the optimization of the heat transfer rate. With a desirability rating of 99.98%, it is estimated in Table 9 and 10 that the maximum value of $\mathrm{Re}_x^{-\frac{1}{2}}\mathrm{Nu}_x$ for water-SWCNT is 0.880135 and 0.683066 for water-MWCNT, achieved when $M = 0.05$, $\varphi = 0.2$ and $\gamma = 0.01$. The results of the RSM are comparable, showing that SWCNTs produce higher heat transfer than MWCNTs.

Table 9. The desirability optimization of y_{SWCNT}.

Solution	x_1	x_2	x_3	Response fit	Composite desirability
1	1	1	−1	0.880135	0.999800

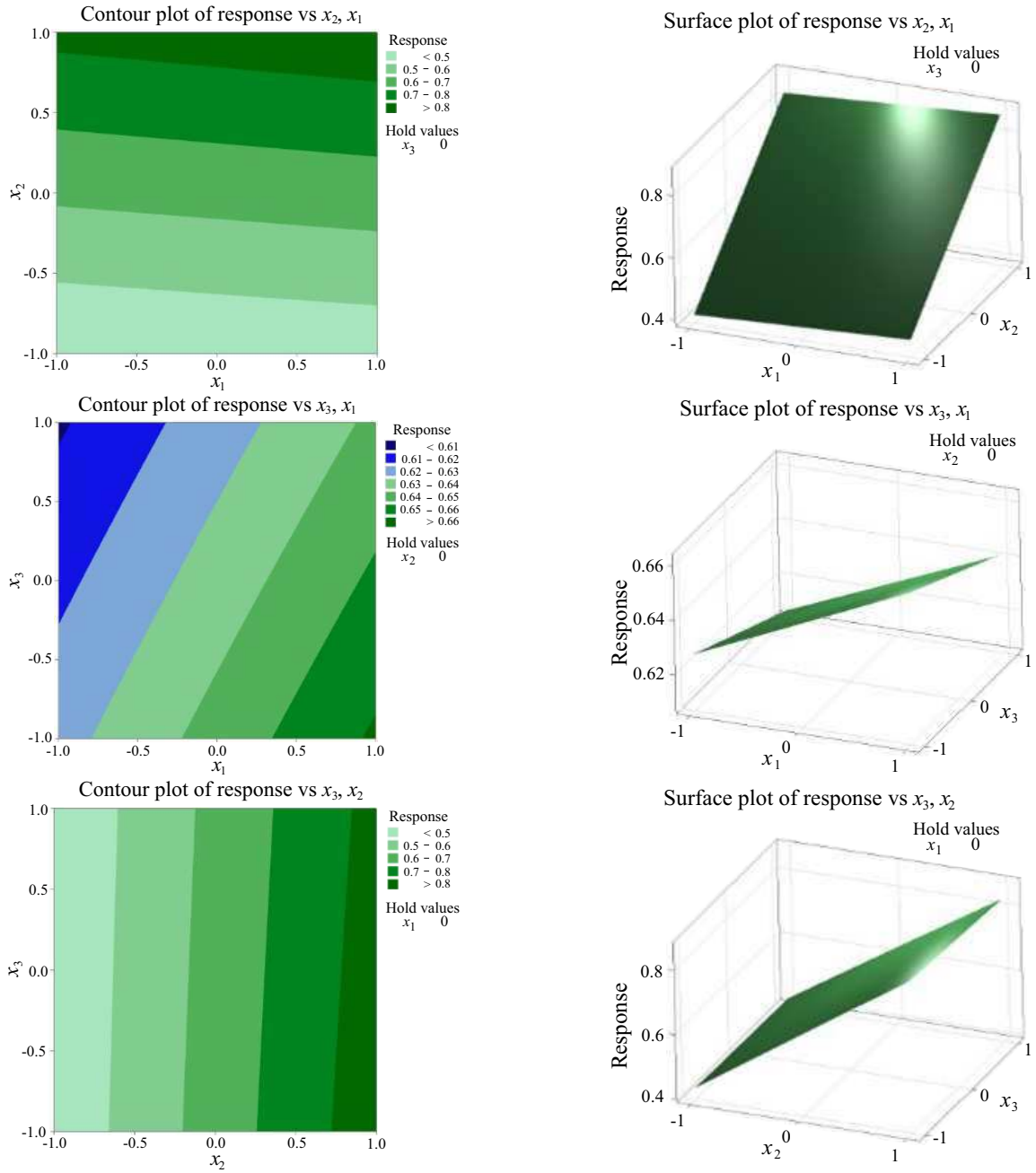

Fig. 11. Contour and surface plots response, $\mathrm{Re}_x^{-\frac{1}{2}}\mathrm{Nu}_x$ with the combination of three parameters (x_1, x_2 and x_3) of y_{SWCNT}.

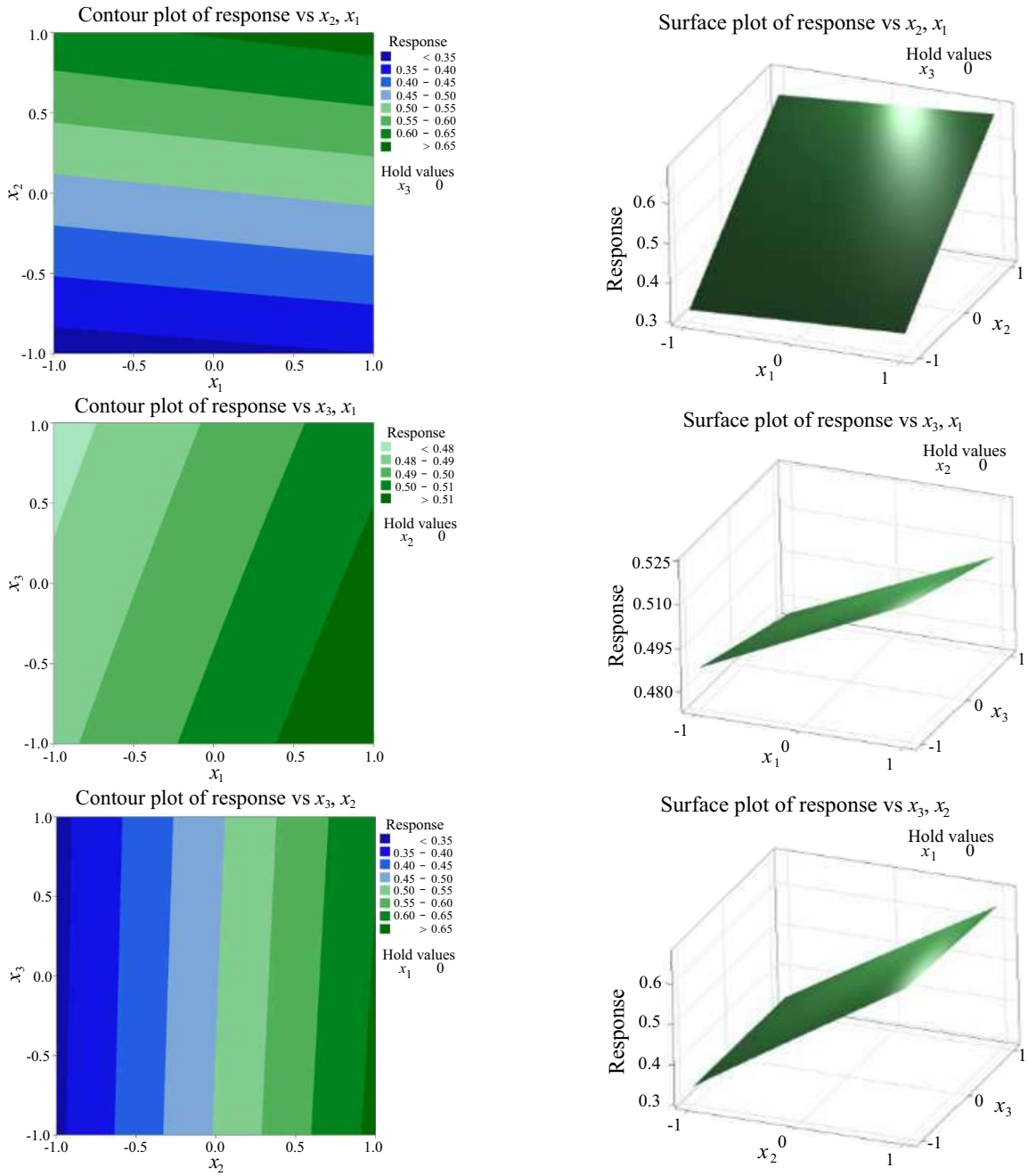

Fig. 12. Contour and surface plots response, $\mathrm{Re}_x^{-\frac{1}{2}}\mathrm{Nu}_x$ with the combination of three parameters (x_1, x_2 and x_3) of y_{MWCNT}.

Table 10. The desirability optimization of y_{MWCNT}.

Solution	x_1	x_2	x_3	Response fit	Composite desirability
1	1	1	−1	0.683066	0.999762

5. Conclusion

The permeable stretching or shrinking cylinder with the influence of hydromagnetic effects on the stagnation point flow in carbon nanotubes has been studied. This study has considered several aspects, including velocity, temperature, skin friction coefficient and local Nusselt number. Consequently, the results of the current study are presented below:

1. The dual solutions exist for the shrinking case ($\varepsilon < 0$), whereas unique solutions are obtained for stretching case ($\varepsilon > 0$).
2. Single-wall carbon nanotubes provide a better skin friction coefficient and heat transfer compared to multi-wall carbon nanotubes.
3. Kerosene-based carbon nanotubes contribute to a higher skin friction coefficient, whereas water-based carbon nanotubes enhance heat transfer.
4. The increment on value of γ and M results in higher skin friction coefficient and heat transfer rate.
5. The nanoparticle volume fraction, φ, positively impacts the rate of heat transfer. The maximum Nusselt number, estimated at 0.880135 with a desirability of 99.98%, is obtained for water-SWCNT at $M = 0.05$, $\varphi = 0.2$ and $\gamma = 0.01$.

[1] Wang C. Y. Fluid flow due to a stretching cylinder. Physics of Fluids. **31** (3), 466–468 (1988).

[2] Mukhopadhyay S. MHD boundary layer slip flow along a stretching cylinder. Ain Shams Engineering Journal. **4** (2), 317–324 (2013).

[3] Najib N., Bachok N., Arifin N. M., Ishak A. Stagnation point flow and mass transfer with chemical reaction past a stretching/shrinking cylinder. Scientific Reports. **4** (1), 4178 (2014).

[4] Mishra U., Singh G. Dual solutions of mixed convection flow with momentum and thermal slip flow over a permeable shrinking cylinder. Computers & Fluids. **93**, 107–115 (2014).

[5] Mat N. A. A., Arifin N. M., Nazar R., Bachok N. Boundary layer stagnation-point slip flow and heat transfer towards a shrinking/stretching cylinder over a permeable surface. Applied Mathematics. **6** (3), 466–475 (2015).

[6] Khashi'ie N. S., Waini I., Zainal N. A., Hamzah K., Kasim A. R. K. Hybrid nanofluid flow past a shrinking cylinder with prescribed surface heat flux. Symmetry. **12** (9), 1493 (2020).

[7] Awaludin I. S., Ahmad R., Ishak A. On the stability of the flow over a shrinking cylinder with prescribed surface heat flux. Propulsion and Power Research. **9** (2), 181–187 (2020).

[8] Kardri M. A., Bachok N., Arifin N. M., Ali F. M., Rahim Y. F. Magnetohydrodynamic flow past a nonlinear stretching or shrinking cylinder in nanofluid with viscous dissipation and heat generation effect. Journal of Advanced Research in Fluid Mechanics and Thermal Sciences. **90** (1), 102–114 (2022).

[9] Choi S. U., Eastman J. A. Enhancing thermal conductivity of fluids with nanoparticles (No. ANL/MSD/CP-84938; CONF-951135-29). Argonne National Lab.(ANL), Argonne, IL (United States), (1995).

[10] Arifin N. M., Nazar R., Pop I. Viscous flow due to a permeable stretching/shrinking sheet in a nanofluid. Sains Malaysiana. **40** (12), 1359–1367 (2011).

[11] Wang C. Y. Stagnation flow towards a shrinking sheet. International Journal of Non-Linear Mechanics. **43** (5), 377–382 (2008).

[12] Tiwari R. K., Das M. K. Heat transfer augmentation in a two-sided lid-driven differentially heated square cavity utilizing nanofluids. International Journal of heat and Mass transfer. **50** (9–10), 2002–2018 (2007).

[13] Bachok N., Ishak A., Pop I. Boundary-layer flow of nanofluids over a moving surface in a flowing fluid. International Journal of Thermal Sciences. **49** (9), 1663–1668 (2010).

[14] Makinde O. D., Aziz A. Boundary layer flow of a nanofluid past a stretching sheet with a convective boundary condition. International Journal of Thermal Sciences. **50** (7), 1326–1332 (2011).

[15] Bachok N., Ishak A., Pop I. Unsteady boundary-layer flow and heat transfer of a nanofluid over a permeable stretching/shrinking sheet. International Journal of Heat and Mass Transfer. **55** (7–8), 2102–2109 (2012).

[16] Bachok N., Ishak A., Nazar R., Senu N. Stagnation-point flow over a permeable stretching/shrinking sheet in a copper-water nanofluid. Boundary Value Problems. **2013**, 39 (2013).

[17] Iijima S. Helical microtubules of graphitic carbon. Nature. **354** (6348), 56–58 (1991).

[18] Halelfadl S., Maré T., Estellé P. Efficiency of carbon nanotubes water based nanofluids as coolants. Experimental Thermal and Fluid Science. **53**, 104–110 (2014).

[19] Anuar N. S., Bachok N., Arifin N. M., Rosali H. MHD flow past a nonlinear stretching/shrinking sheet in carbon nanotubes: Stability analysis. Chinese Journal of Physics. **65**, 436–446 (2020).

[20] Mahapatra T. R., Gupta A. S. Magnetohydrodynamic stagnation-point flow towards a stretching sheet. Acta Mechanica. **152** (1), 191–196 (2001).

[21] Aman F., Ishak A., Pop I. Magnetohydrodynamic stagnation-point flow towards a stretching/shrinking sheet with slip effects. International Communications in Heat and Mass Transfer. **47**, 68–72 (2013).

[22] Ishak A., Nazar R., Pop I. Magnetohydrodynamic (MHD) flow of a micropolar fluid towards a stagnation point on a vertical surface. Computers & Mathematics with Applications. **56** (12), 3188–3194 (2008).

[23] Uddin Z., Kumar M. MHD Heat and Mass Transfer Free Convection Flow near The Lower Stagnation Point of an Isothermal Cylinder Imbedded in Porous Domain with the Presence of Radiation. Jordan Journal of Mechanical & Industrial Engineering. **5** (5), 419–423 (2011).

[24] Uddin Z., Kumar M. Hall and ion-slip effect on MHD boundary layer flow of a micro polar fluid past a wedge. Scientia Iranica. **20** (3), 467–476 (2013).

[25] Uddin Z., Kumar M., Harmand S. Influence of thermal radiation and heat generation/absorption on MHD heat transfer flow of a micropolar fluid past a wedge considering hall and ion slip currents. Thermal Science. **18** (suppl. 2), 489–502 (2014).

[26] Sama N. A. A., Bachok N., Arifin N. M. The significant effect of hydromagnetic on carbon nanotubes based nanofluids flow and heat transfer past a porous stretching/shrinking sheet. Journal of Advanced Research in Fluid Mechanics and Thermal Sciences. **106** (1), 51–64 (2023).

[27] Anuar N. S., Bachok N., Arifin N. M., Rosali H. Stagnation point flow and heat transfer over an exponentially stretching/shrinking sheet in CNT with homogeneous–heterogeneous reaction: stability analysis. Symmetry. **11** (4), 522 (2019).

[28] Norzawary N. H. A., Bachok N., Ali F. M., Arifin N. M. Slip Flow Over an Exponentially Stretching/Shrinking Sheet in a Carbon Nanotubes with Heat Generation: Stability Analysis. Journal of Advanced Research in Fluid Mechanics and Thermal Sciences. **108** (1), 28–38 (2023).

[29] Shirvan K. M., Mamourian M., Mirzakhanlari S., Ellahi R., Vafai K. Numerical investigation and sensitivity analysis of effective parameters on combined heat transfer performance in a porous solar cavity receiver by response surface methodology. International Journal of Heat and Mass Transfer. **105**, 811–825 (2017).

[30] Mahanthesh B., Shehzad S. A., Mackolil J., Shashikumar N. S. Heat transfer optimization of hybrid nanomaterial using modified Buongiorno model: A sensitivity analysis. International Journal of Heat and Mass Transfer. **171**, 121081 (2021).

[31] Mahanthesh B., Thriveni K., Rana P., Muhammad T. Radiative heat transfer of nanomaterial on a convectively heated circular tube with activation energy and nanoparticle aggregation kinematic effects. International Communications in Heat and Mass Transfer. **127**, 105568 (2021).

[32] Yahaya R I., Mustafa M. S., Arifin N. M., Pop I., Ali F. M., Isa S. S. P. M. Hybrid nanofluid flow past a biaxial stretching/shrinking permeable surface with radiation effect: Stability analysis and heat transfer optimization. Chinese Journal of Physics. **85**, 402–420 (2023).

[33] Othman M. N., Jedi A., Bakar N. A. A. MHD Stagnation Point on Nanofluid Flow and Heat Transfer of Carbon Nanotube over a Shrinking Surface with Heat Sink Effect. Molecules. **26** (24), 7441 (2021).

[34] Alhadri M., Raza J., Yashkun U., Lund L. A., Maatki C., Khan S. U., Kolsi L. Response surface methodology (RSM) and artificial neural network (ANN) simulations for thermal flow hybrid nanofluid flow with Darcy-Forchheimer effects. Journal of the Indian Chemical Society. **99** (8), 100607 (2022).

Потік у пограничному шарі та теплопередача до циліндра, що розтягується або стискається, всередині вуглецевих нанотрубок з гідромагнітними ефектами

Сідін А. А. А.[1], Бачок Н.[2], Вахід Н. С.[2], Мустафа М. С.[2]

[1]*Інститут математичних досліджень, Університет Путра Малайзія, 43400 UPM Серданг, Селангор, Малайзія*

[2]*Кафедра математики та статистики, Факультет природничих наук, Університет Путра Малайзія, 43400 UPM Серданг, Селангор, Малайзія*

Розглянуто числове дослідження потоку точки застою повз циліндр, що розтягується або стискається, у вуглецевих нанотрубках за наявності гідромагнітних ефектів. Це дослідження було розв'язано за допомогою звичайних диференціальних рівнянь, отриманих за допомогою перетворення подібності, яке трансформувалося з основних рівнянь разом з граничними умовами, а потім реалізовано за допомогою розв'язувача bvp4c на програмній платформі MATLAB, що забезпечує точні результати. Розглядаються два типи базових рідин, а саме: вода та гас. Також у цьому дослідженні використовуються одностінні та багатостінні типи вуглецевих нанотрубок, причому одностінні та багатостінні мають різні значення густини. Дослідження проводиться шляхом побудови графіків швидкості, температури, коефіцієнта поверхневого тертя та швидкості теплопередачі. Розглянуто декілька параметрів, таких як магнітне поле M, параметр кривизни γ, параметр розтягування або стискання ε та об'ємна частка наночастинок φ. На основі числових результатів показано, що для параметра стискання існує неєдиний розв'язок, тоді як для параметра розтягування отримано єдиний розв'язок. Крім того, було виявлено, що одностінні вуглецеві нанотрубки та нанорідина на основі гасу є ефективнішими для теплопередачі, ніж багатостінні вуглецеві нанотрубки та нанорідина на основі води. Для оптимізації теплопередачі використовується методологія поверхневого відгуку (RSM), при цьому максимальна теплопередача для системи "вода–SWCNT" оцінюється в 0.880135, а бажана кількість становить 99.98%, що вище, ніж для системи "вода–MWCNT", що вказує на більшу ефективність системи "вода–SWCNT".

Ключові слова: *теплопередача; розтягування або стиснення циліндра; вуглецеві нанотрубки; оптимізація; подвійні розв'язки.*